A novel Hsp90 phospho-switch modulates virulence in the major human fungal pathogen *Candida albicans*

Leenah Alaalm[1], Julia L. Crunden[1,2], Mark Butcher[3], Ulrike Obst[2], Ryann Whealy[2], Carolyn E. Williamson[1], Heath E. O'Brien[4], Christiane Schaffitzel[5], Gordon Ramage[3] and Stephanie Diezmann[1,2*]

[1] Department of Biology & Biochemistry, University of Bath, Bath, United Kingdom

[2] School of Cellular and Molecular Medicine, University of Bristol, Bristol, United Kingdom

[3] School of Medicine, Dentistry and Nursing, University of Glasgow, Glasgow, United Kingdom

[4] MRC Centre for Neuropsychiatric Genetics & Genomics, Division of Psychological Medicine & Clinical Neurosciences, Cardiff University, Cardiff, United Kingdom

[5] School of Biochemistry, University of Bristol, Bristol, United Kingdom

Leenah Alaalm and Julia L. Crunden contributed equally to this work.

Running title: Hsp90 phosphorylation modulates *Candida albicans* virulence

The ubiquitous molecular chaperone Hsp90 is a key regulator of cellular proteostasis and environmental stress responses. Hsp90 also regulates cellular morphogenesis, drug resistance, and virulence in human pathogenic fungi, which kill more than 1.6 million patients each year worldwide. Invasive fungal infections are difficult to treat due to the lack of effective antifungal therapies, resulting in mortality rates of up to 95%. As a key regulator of fungal virulence, Hsp90 is an attractive therapeutic target. However, fungal and animal homologs are highly conserved, impeding fungal-specific targeting. Thus, understanding the factors that regulate Hsp90 could provide an alternative strategy aimed at exclusively targeting this regulator of fungal virulence. Here, we demonstrate how CK2-mediated phosphorylation of two Hsp90 residues modulates virulence in a major fungal pathogen of humans, *Candida albicans*. We combined proteomics, molecular evolution and structural modelling with molecular biology to identify and characterize two Hsp90 phosphorylation sites. Phosphorylation negatively affects thermal stress response, morphogenesis, drug susceptibility and fungal virulence. Our results provide the first record of specific Hsp90 phosphorylation sites acting as modulators of fungal virulence. Post-translational modifications of Hsp90 could prove valuable in future exploitation as antifungal drug targets.

Fungi kill as many patients as tuberculosis and about three times as many as malaria each year[1]. One of the most deadly fungal pathogens, *Candida albicans* causes ~750,000 cases of invasive life-threatening bloodstream infections in immunocompromised patients worldwide each year[1], with mortality rates approaching 75%[2]. In addition to high burdens on human life, fungal infections put a significant strain on health care costs. The United States alone spent $4.5 billion on 75,055 hospitalizations necessitated by fungal disease over ten years[3] while English NHS trusts spend annually approximately £90 million on antifungal drugs[4]. This already dire situation is further exacerbated by the ever-growing number of patients at risk of contracting invasive fungal infections. It is thus imperative to understand the biological principles underpinning fungal virulence to identify points of fragility suitable for therapeutic targeting.

Diverse aspects of fungal pathogenicity are controlled by heat shock protein 90 (Hsp90), a ubiquitous regulator of the cellular protein homeostasis. Hsp90 regulates cell morphology, drug resistance, and virulence in *C. albicans*[5] and other leading fungal

57 pathogens of humans *Cryptococcus neoformans*[6], which causes brain infections and
58 *Aspergillus fumigatus*[7] which targets the lungs, as well as the dermatophyte *Trichophyton*
59 *rubrum*[8], and *Sporothrix schenckii*[9], the causative agent of cutaneous infections. Hsp90's role
60 in virulence and development is best understood in *C. albicans,* where pharmacological
61 inhibition or genetic reduction of Hsp90 result in reduced drug resistance in planktonic cells[5]
62 and biofilms[10], switching to filamentous growth[11], induction of same-sex mating[12], and
63 delayed cell cycle progression[13]. Although attractive as a drug target for its role in fungal
64 virulence, Hsp90 is highly conserved between mammals and fungi[14]. High sequence
65 conservation prohibits specific targeting of fungal Hsp90 and resulted in severe host toxicity
66 when mice infected with *C. albicans* where treated with Hsp90 inhibitors developed as anti-
67 cancer therapeutics and antifungal drugs[15]. Thus, understanding fungal-specific regulatory
68 mechanisms of Hsp90 could provide an alternative therapeutic approach and is consequently
69 of biological and clinical relevance.

70 Post-translational modifications (PTMs) play a crucial role in regulating Hsp90. Their
71 impact on chaperone activity, directionality of the chaperone cycle, and binding to co-
72 chaperones have been extensively studied in mammalian cells and the model eukaryote
73 *Saccharomyces cerevisiae*[16]. However, examples of Hsp90 PTMs in pathogenic fungi are
74 limited to the observations that concurrent acetylation of two lysine residues, K30 and K271,
75 resulted in increased susceptibility to Hsp90 inhibition, morphogenetic alterations, and
76 impaired macrophage pyroptosis in *C. albicans*[17], as well as attenuated virulence in *A.*
77 *fumigatus*[18]. Given the importance of kinases as drug targets[19] and experimental evidence of
78 phosphorylation regulating most Hsp90 activities, this type of PTM is of particular interest.
79 Phosphorylation negatively affects the chaperone cycle, interactions with clients and co-
80 chaperones, conformational switching, and sensitivity to Hsp90 inhibitors[20]. The ubiquitous
81 tetrameric casein kinase 2 (CK2), one of several kinases targeting Hsp90, phosphorylates
82 $Hsp90^{T36}$ in mammalian cells and $Hsp90^{T22}$ in *S. cerevisiae*. This highly conserved residue
83 was initially identified as critical for the survival of elevated temperatures[21] and
84 phosphorylation of $T^{22/36}$ reduces kinase client stability and co-chaperone binding[22]. In *C.*
85 *albicans*, CK2 phosphorylates Hsp90 serine and threonine residues[23]. Yet, specific Hsp90
86 residues targeted by CK2 and the functional consequences thereof have not been found.

87 Here we demonstrate that CK2-mediated phosphorylation of the newly identified Hsp90
88 residue S530 blocks *C. albicans* virulence and expression of virulence-related traits, such as
89 cellular morphogenesis and survival of thermal stress. Probing the conserved T22 residue

90 revealed that any alteration of this residue leads to loss of Hsp90 function. Our results
91 emphasize the importance of Hsp90 phospho-regulation in fungal virulence and provide a
92 potential site for future therapeutic targeting.
93
94 **Results**
95 **Mapping, modeling, and evolutionary history of CK2 Hsp90 phosphorylation sites.** To
96 map CK2 phosphorylation sites in *C. albicans* Hsp90 *in situ*, the wild-type strain and four
97 mutants, each lacking one CK2 subunit (for strain construction see Tables S1, S2, S3, and
98 Supplementary Information), were grown in rich media at 30˚C upon which epitope tagged
99 Hsp90 was purified and analyzed by mass spectrometry. Without further enrichment, Hsp90
100 sequence coverage in trypsin digests was 70% or higher and ranged between 40-45% in
101 endoproteinase Glu-C digests. Three phosphorylation sites were identified (Table 1). S279
102 was only phosphorylated in the *cka1*Δ/Δ mutant. S294 was phosphorylated in the wild type
103 and all four CK2 mutants. S530 was phosphorylated in the wild type, the *cka1*Δ/Δ and the
104 *ckb1*Δ/Δ mutants, but not the *cka2*Δ/Δ and *ckb2*Δ/Δ mutants. Interestingly, deletion of *CKA2*
105 results in increased fluconazole resistance[24], while Hsp90 inhibition abolishes fluconazole
106 resistance[25].
107 Thus, we hypothesized that phosphorylation of $Hsp90^{S530}$ blocks Hsp90 function,
108 thereby reducing resistance to antifungal drugs. The acquisition of a PTM that reduces drug
109 resistance appears counter-intuitive, but the trade-off theory of optimal virulence predicts
110 selective pressure to evolve reduced virulence in cases where the host and pathogen's fitness
111 are aligned[26]. *C. albicans's* primary ecological niche is as a commensal on mucosal surfaces
112 of the oral cavity and GI tract. To test this, we assessed the effect of $Hsp90^{S530}$
113 phosphorylation on diverse virulence traits, including high temperature growth and
114 morphogenesis.
115 In addition to investigating S530, we decided to also characterize the conserved CK2
116 target $Hsp90^{T22/T36}$, whose *C. albicans* homolog is T25, called T25 henceforth. T25 resides in
117 a highly conserved region of Hsp90's N-terminus, which contains the ATP binding site and is
118 the target of the Hsp90 inhibitors geldanamycin and radicicol[27]. S530 is located in a highly
119 divergent region of the Hsp90 middle domain, where client proteins bind[27] (Fig. 1a). To
120 elucidate the relationship of these two residues within the Hsp90 molecule, we modeled the
121 full-length *C. albicans* Hsp90 monomer on the *S. cerevisiae* crystal structure[28] (Fig. 1b). A
122 total of 609 residues (94% coverage) were aligned with 100% confidence, sharing 89%

123 identity between both yeast species. The homology model revealed that both residues are
124 located in loop regions without secondary structural elements (Fig. 1b). T25 resides in close
125 proximity to the ATP binding pocket, while S530 is located in a loop near the protein's C-
126 terminus. The surface model shows that T25, although not a hydrophobic amino acid, is not
127 solvent exposed, while S530 is (Fig. 1b). These observations are in keeping with molecular
128 evolution theory, which predicts that decreased solvent accessibility results in fewer amino
129 acid polymorphisms[29] and thus higher sequence conservation.

130 Given the divergent nature of the S530 residue (Fig. 1a), we investigated its
131 evolutionary history within the fungal kingdom, asking if *C. albicans* presented a unique case
132 or if multiple transitions could be detected. Aligning 659 amino acids of 240 fungal Hsp90
133 sequences, representing nine sub-phyla, with the murine homolog Hsp90ab1 revealed serine
134 to be a derived allele originating at least eleven times independently within the Dikarya,
135 which encompass the Ascomycota and Basidiomycota, and represent ~96% of known fungal
136 species[30] (Fig. 1c, S1, Table S4). Basal fungi, such as the Chytridiomycota, share an aspartic
137 acid allele with animal cytosolic Hsp90. Threonine originated in the last common ancestor of
138 the Dikarya and threonine to serine transitions were detected in five of the six sub-phyla.
139 Serine alleles were detected in species considered plant pathogens (*Ustilago hordei*, *Puccinia*
140 complex, *Aspergillus niger, Ashbya gossypii*), species associated with trees (*Neolecta*
141 *irregularis*), fermentative yeast (*Nadsonia fulvescens*), methylotrophic yeasts *(Komagataella*
142 *phaffi*, *K. pastoris*, *Ogataea parapolymorpha*, *O. polymorpha*), halo-tolerant species
143 (*Debaryomyces hansenii, Zygosaccharomyces rouxii*) and the opportunistic pathogens
144 (*Meyerozyma guilliermondii*, *Malassezia globosa*, *Candida parapsilosis*). No serine alleles
145 were detected amongst the 82 Agaromycotina, which include the human pathogen
146 *Cryptococcus neoformans* as well as mushrooms and jelly fungi. In summary, the serine allele
147 is rare; it is present in less than 5% of fungi. Serine occurs in species that are capable of
148 causing disease in plants, thrive in extreme environments, and exist as commensals of the
149 human body where they can cause opportunistic infections in responses to changes in the
150 host's immune status, like *C. albicans*.

151 **Hsp90 phosphorylation negatively affects protein stability and co-chaperone binding.** To
152 investigate the effects of phosphorylation of T25 and S530 and to accommodate the 'obligate
153 diploid' nature of *C. albicans*, we generated strains expressing one mutant *hsp90* allele, where
154 the relevant residue was replaced with either a phosphomimetic glutamic acid (E) or a non-
155 phosphorylatable alanine (A) while the remaining *HSP90* wild-type allele was placed under

156 the control of the maltose-inducible promoter *MAL2*p (Tables S1, S2, S3, Supplementary
157 Information). Consequently, strains grown in dextrose solely expressed the mutant allele,
158 thereby revealing the effects of phosphorylation. Growth in maltose resulted in expression of
159 the wild-type allele, serving as control and for strain maintenance. Non-phosphorylatable and
160 phosphomimetic alleles were created for both residues (T25A, T25E, S530A, S530E) and
161 compared to the wild type and the *MAL2-HSP90* promoter control, that carries two *HSP90*
162 wild-type alleles, one of which is under the control of the *MAL2* promoter.

163 To test if phosphorylation affects Hsp90 stability, strains were grown in dextrose or
164 maltose and cell extracts probed for Hsp90 using an antibody that recognizes amino acid
165 residues 693-702 in the *C. albicans* Hsp90 C-terminus[31]. Replacing T25 or S530 with the
166 phosphomimetic residue (E) almost completely depleted Hsp90 levels in cells grown in
167 dextrose when compared to the *MAL2-HSP90* control. Protein levels remained comparable in
168 the strains carrying the non-phosphorylatable alanine allele (A) (Fig. 2a). Thus,
169 phosphorylation of T25 or S530 destabilizes Hsp90.

170 Given the importance of T22/T36 for co-chaperone binding in *S. cerevisiae* and
171 mammalian cells[32], we aimed to determine if the homologous T25 residue plays a similar role
172 in *C. albicans*. Cell lysates from strains with TAP or HA tagged co-chaperones were
173 immunoprecipitated with IgG or α-HA agarose and probed for presence of co-chaperones
174 Cdc37, Aha1, Sba1, and Sti1, which bind to Hsp90's N-terminal domain[33], and for co-
175 immunoprecipitated Hsp90 (Fig. 2b). Changing T25 to either a phosphomimetic or non-
176 phosphorylatable form severely reduced binding of Hsp90 to all four co-chaperones,
177 indicating functional conservation of T25 with regards to co-chaperone binding.

178 **Hsp90 phosphorylation blocks expression of key virulence traits.** Mutational analysis of
179 the *S. cerevisiae* homolog *HSP82* revealed T22 to be essential for survival of elevated
180 temperatures[34], a key virulence trait. To determine the importance of T25 and S530 for
181 growth at high temperatures in *C. albicans*, *hsp90* mutants as well as the wild-type and
182 promoter control strains were spotted onto medium containing either dextrose or maltose and
183 exposed to different temperatures (Fig. 3a). Although neither T25 mutant grew as robust as
184 the wild type or the *MAL2-HSP90* control, the phosphomimetic T25E grew better than the
185 non-phosphorylatable T25A at temperatures above 25˚C. Single colonies were detectable for
186 T25E at the highest dilutions even at 37˚C and 39˚C. Growth of T25A was only detectable at
187 the lowest dilutions at elevated temperatures. In either strain, however, colonies were visibly
188 smaller than in the control suggesting reduced growth rate due to alterations of the T25

189 residue. Growth of the non-phosphorylatable S530A mutant was comparable to the control
190 strains but the phosphomimetic S530E mutant grew much less robust especially at lower
191 temperatures. This suggests phosphorylation of T25 and S530 plays different roles during
192 exposure to thermal stress. Phosphorylation of T25 is required for survival of high
193 temperatures, while phosphorylation of S530 impairs the cell's ability to cope with lower
194 temperatures.

195 Given the importance of Hsp90 in *C. albicans* antifungal drug resistance and the role of
196 Hsp90 PTMs in susceptibility to pharmacological inhibition of Hsp90 function, we tested the
197 phospho-mutants for susceptibility to the commonly used antifungal drug fluconazole and the
198 Hsp90 inhibitor radicicol. Control and phospho-mutant strains were exposed to drug gradients
199 ranging from either 0-256 µg/ml for fluconazole or 0-25 µg/ml for radicicol. Growth was
200 quantified after 48 hours at 25˚C as optical density revealing that expression of *hsp90* mutant
201 alleles sensitizes *C. albicans* to antifungal drug treatment and Hsp90 inhibition (Fig. 3b).
202 Changing T25 to either a phosphomimetic or non-phosphorylatable allele or expressing the
203 S530 phospho-allele rendered *C. albicans* susceptible to either drug. This suggests Hsp90
204 phosphorylation to be a determinant of drug susceptibility.

205 Cellular morphogenetic diversity is a fundamental element of *C. albicans'* virulence
206 repertoire as the ability to switch between yeast and hyphae is essential for the infectious
207 process[35]. To determine how phosphorylation of T25 or S530 affects cellular morphogenesis,
208 the wild type, the *MAL2-HSP90* control and the *hsp90* mutants were grown in standard non-
209 filament inducing conditions in rich media at 30˚C. Microscopic examination of planktonic
210 cells showed robust hyphal growth in both T25 mutants as well as the S530E strain in media
211 containing dextrose, but not maltose (Fig. 3c). To quantify these observations, we calculated
212 the morphology index (MI) for 100 randomly selected cells for each strain (Fig. S2). An MI >
213 1 is indicative of cell elongation or hyphal growth. MI scores for cells grown in dextrose or
214 maltose differed significantly for both T25 mutants and S530E. In maltose, MIs clustered
215 below 1, in dextrose MIs ranged from ~0.2 to ~75. Hence, both T25 mutant alleles and the
216 phosphomimetic S530E allele cause cells to switch from yeast to hyphal growth.

217 **Hsp90's phosphorylation status affects colony appearance and biofilm viability.**
218 Following up on the observation that differential Hsp90 phosphorylation results in elongated
219 cell shape, we assessed macroscopic changes to colony morphology and response to cell wall
220 stress. To capture changes in colony morphology, all strains were grown on nutrient-limited
221 RPMI, synthetic defined (SD) media alone and supplemented with Calcofluor White or

222 Congo Red as well as Spider media, which induces the yeast-to-hyphae transition (Table S5).
223 Upon visual inspection of plates grown for 48 hours at 30˚C, wild-type colonies were
224 indistinguishable from the *MAL2-HSP90* control (Fig. 4). Colonies for both T25 mutants and
225 the S530E strain appeared different from controls on RPMI and SD media. Despite being
226 highly filamentous on a cellular level, colonies of these strains lost their hyphal edge on
227 RPMI. On SD, these colonies were wrinkly rather than smooth. Growth on maltose restored
228 wild type-like growth on RPMI and, to a degree, on SD media. No appreciable differences
229 were observed for colonies grown in the presence of Congo Red or Calcofluor White when
230 compared to SD only media (data not shown). Differences in colony morphology on Spider
231 media appeared to be driven by the carbon source rather than a strain's *HSP90* allele.

232 Morphogenetic diversity is a key prerequisite for the formation of *C. albicans* biofilms,
233 which are medically relevant for two reasons. First, biofilms act as reservoirs that
234 continuously feed the infection, and secondly they are intrinsically resistant to treatment with
235 antifungal drugs[36]. To determine if Hsp90's phosphorylation status affects the intricate
236 developmental program underlying biofilm formation, cells were grown in standard biofilm-
237 inducing conditions in RPMI (2 g/l glucose) at 37˚C. Mature biofilms were imaged using
238 scanning electron microscopy and their cell viability and biomass were quantified employing
239 spectrometric approaches. Microscopic analysis of biofilm architecture at 800x and 8,000x
240 magnifications showed that control strains and phospho-mutants form structurally similar
241 biofilms, suggesting that Hsp90's phosphorylation status does not fundamentally affect
242 overall biofilm development in the conditions tested (Fig. 5a). More detailed inspection of
243 biomass production and cell viability revealed that the latter is significantly decreased in the
244 S530E mutant ($p=0.00205$) relative to the *MAL2-HSP90* control (Fig. 5b, c). This is in
245 keeping with previous observations of phosphorylation of $Hsp90^{S530}$ resulting in a loss-of-
246 function phenotype. All other phospho-mutants displayed significant increases in cell viability
247 (T25A: $p=4.01x10^{-14}$; T25E: $p=9.94x10^{-13}$; S530A: $p=8.68x10^{-7}$). While deviating from our
248 observation of a growth defect in the T25 mutants at 37˚C on YPD agar, Azadmanesh *et al.*
249 have shown that the physical environment influences *C. albicans* gene expression and
250 development[37].

251 Building on our finding that Hsp90's phosphorylation status determines its effect on *C.*
252 *albicans* cellular morphogenesis, we demonstrated that phosphorylation of S530 results in
253 changes in colony morphology and reduced biofilm cell viability due to loss of Hsp90

254 function. Any manipulation of the T25 residue, however, leads to elongated cells, aberrant
255 colony morphology and increased biofilm cell viability.

256 **S530 regulates *C. albicans* virulence in an invertebrate model of fungal pathogenesis.**
257 Once we established the importance of phosphorylation of S530 and T25 in virulence-relevant
258 traits using different *in vitro* assays, we aimed to determine if and how Hsp90
259 phosphorylation affects fungal virulence. To test this, *Manduca sexta* caterpillars, an
260 invertebrate model host of fungal disease[38], were infected with 10^7 yeast cells. Caterpillar
261 survival was then assessed in groups of ten after 16 hours of incubation at the physiologically
262 relevant temperature of 37˚C. Strain S530E displayed significantly reduced virulence
263 compared to the *MAL2-HSP90* control (Table S6). Nine caterpillars infected with S530E
264 survived compared to two caterpillars infected with *MAL2-HSP90* (p=0.0054775). Thus,
265 S530 phosphorylation blocks Hsp90 function, thereby attenuating virulence in an animal host.

266 In summary, Hsp90's phosphorylation status affects fungal virulence. Taken together,
267 our results suggest that S530 is a novel phospho-switch. When phosphorylated, it blocks
268 Hsp90 function and thus the expression of virulence traits, which may aid its adaptation to a
269 commensal lifestyle while maintaining the ability to cause invasive infections. Alterations of
270 T25, however, are important beyond phosphorylation, suggesting this residue to be a 'switch
271 point', important for structural integrity of *C. albicans* Hsp90.

272

273 **Discussion**

274 Our data indicate that CK2-mediated phosphorylation of $Hsp90^{S530}$ blocks expression of
275 virulence traits in a major human pathogen while any alteration of $Hsp90^{T25}$ resulted in a loss-
276 of-function phenotype. This suggests that S530 is a novel *C. albicans* Hsp90 phospho-switch
277 while T25 acts as switch point.

278 Similarly, to what has been observed in *S. cerevisiae* and mammalian cells, any
279 modification of *C. albicans* T25 negatively affects co-chaperone binding, survival of high
280 temperatures, and susceptibility to drug and Hsp90 inhibition[32,39]. We thus propose that T25
281 acts as a switch point in *C. albicans* Hsp90. Switch points impact on the overall conformation
282 and function of a protein through conformational disturbances altering chaperone function[40].
283 These types of allosteric PTMs are of evolutionary significance as they expand the
284 proteome's complexity and facilitate dynamic responses to a large number of stimuli without
285 the need for additional genes[41]. The effect, however, appears to be restricted to T22 in *S.*
286 *cerevisiae* and T25 in *C. albicans*, as changes in the acetylation status of the neighboring

287 conserved *C. albicans* K30[17] or *S. cerevisiae* K27[42] residues did not result in loss of Hsp90
288 function.

289 Detection of phosphorylation of S530 has remained rather elusive. Only one[43] of five
290 global phospho-proteomic analyses of *C. albicans*[44-47] detected phosphorylation of Hsp90^{S530}
291 in *C. albicans* hyphal cells[43]. This finding is consistent with our experimental data showing
292 filamentous growth in the phosphomimetic S530E mutant. While our proteomic analysis
293 revealed S530 to be phosphorylated in the wild type, the wild-type and *MAL2-HSP90* control
294 are phenotypically more similar non-phosphorylatable mutant S530A than the they are to
295 phosphomimetic mutant S530E (Fig. 3). This would suggest that phosphorylation of S530 is
296 sparsely deployed and dynamic. Characterizing the *S. cerevisiae* homologous residue T533
297 using phosphomimetic and non-phosphorylatable alleles revealed that this residue does not
298 affect survival at elevated temperatures, susceptibility to Hsp90 inhibition, or yeast growth[48]
299 suggesting evolutionary divergence in sequence and function. Taken together, the dynamic
300 phosphorylation status of S530 carefully orchestrating *C. albicans* virulence in a commensal
301 turned pathogen yeast and the lack of involvement in Hsp90 function of T533 in the benign
302 yeast *S. cerevisiae* would be in keeping with S530 to be a genetic factor that reduces severity
303 as predicted by the trade-off hypothesis of optimal virulence theory.

304 In conclusion, Hsp90's phosphorylation status and structural integrity affect fungal
305 virulence. CK2-mediated phosphorylation of the divergent S530 residue resulting in reduced
306 fungal virulence could be further exploited as a novel therapeutic target to fight fungal
307 infections.

308

309 **References**

310 1. Bongomin, F., Gago, S., Oladele, R. & Denning, D. Global and multi-national
311 prevalence of fungal diseases - estimate precision. *JoF* **3,** 57–29 (2017).
312 2. Brown, G. D. *et al.* Hidden killers: Human fungal infections. *Sci Transl Med* **4,**
313 165rv13 (2012).
314 3. Benedict, K., Jackson, B. R., Chiller, T. & Beer, K. D. Estimation of direct healthcare
315 costs of fungal diseases in the United States. *Clin Infect Dis* **30,** 1 (2018).
316 4. Whitney, L. *et al.* Effectiveness of an antifungal stewardship programme at a London
317 teaching hospital 2010–16. *J Antimicrob Chemother* **74,** 234–241 (2018).
318 5. Singh, S. D. *et al.* Hsp90 governs echinocandin resistance in the pathogenic yeast
319 *Candida albicans* via calcineurin. *PLoS Pathog* **5,** e1000532 (2009).
320 6. Cordeiro, R. de A. *et al.* Inhibition of heat shock protein 90 enhances the susceptibility
321 to antifungals and reduces the virulence of *Cryptococcus neoformans*/*C. gattii* species
322 complex. *Microbiology* **162,** 309–317 (2015).

323 7. Lamoth, F., Juvvadi, P. R., Fortwendel, J. R. & Steinbach, W. J. Heat shock protein 90
324 is required for conidiation and cell wall integrity in *Aspergillus fumigatus*. *Eukaryot*
325 *Cell* **11,** 1324–1332 (2012).
326 8. Jacob, T. R. *et al.* Heat shock protein 90 (Hsp90) as a molecular target for the
327 development of novel drugs against the dermatophyte *Trichophyton rubrum*. *Front*
328 *Microbiol* **6,** 330–10 (2015).
329 9. Rodriguez-Caban, J., Gonzalez-Velazquez, W., Perez-Sanchez, L., Gonzalez-Mendez,
330 R. & Valle, N. R.-D. Calcium/calmodulin kinase1 and its relation to thermotolerance
331 and HSP90 in *Sporothrix schenckii*: an RNAi and yeast two-hybrid study. *BMC*
332 *Microbiol* **11,** 162 (2011).
333 10. Robbins, N. *et al.* Hsp90 governs dispersion and drug resistance of fungal biofilms.
334 *PLoS Pathog* **7,** e1002257 (2011).
335 11. Shapiro, R. S. *et al.* Hsp90 orchestrates temperature-dependent *Candida albicans*
336 morphogenesis via Ras1-PKA signaling. *Curr Biol* **19,** 621–629 (2009).
337 12. Guan, G. *et al.* Environment-induced same-sex mating in the yeast *Candida albicans*
338 through the Hsf1–Hsp90 pathway. *PLoS Biol.* **17,** e2006966–25 (2019).
339 13. Senn, H., Shapiro, R. S. & Cowen, L. E. Cdc28 provides a molecular link between
340 Hsp90, morphogenesis, and cell cycle progression in *Candida albicans*. *Mol Biol Cell*
341 **23,** 268–283 (2012).
342 14. Swoboda, R. K. *et al.* Structure and regulation of the *HSP90* gene from the pathogenic
343 fungus *Candida albicans*. *Infect Immun* **63,** 4506–4514 (1995).
344 15. Cowen, L. E. *et al.* Harnessing Hsp90 function as a powerful, broadly effective
345 therapeutic strategy for fungal infectious disease. *PNAS* **106,** 2818–2823 (2009).
346 16. Mollapour, M. & Neckers, L. Post-translational modifications of Hsp90 and their
347 contributions to chaperone regulation. *BBA* **1823,** 648–655 (2012).
348 17. Li, X., Robbins, N., O'Meara, T. R. & Cowen, L. E. Extensive functional redundancy
349 in the regulation of *Candida albicans* drug resistance and morphogenesis by lysine
350 deacetylases Hos2, Hda1, Rpd3 and Rpd31. *Mol Microbiol* **103,** 635–656 (2016).
351 18. Lamoth, F. *et al.* Identification of a key lysine residue in heat shock protein 90 required
352 for azole and echinocandin resistance in *Aspergillus fumigatus*. *Antimicrob Agents*
353 *Chemother* **58,** 1889–1896 (2014).
354 19. Cohen, P. Protein kinases - the major drug targets of the twenty-first century? *Nat Rev*
355 *Drug Discov* **1,** 309–315 (2002).
356 20. Sima, S. & Richter, K. Regulation of the Hsp90 system. *BBA-Mol Cell Res* **1865,** 889–
357 897 (2018).
358 21. Borkovich, K. A., Farrelly, F. W., Finkelstein, D. B., Taulien, J. & Lindquist, S. hsp82
359 is an essential protein that is required in higher concentrations for growth of cells at
360 higher temperatures. *Mol Cell Biol* **9,** 3919–3930 (1989).
361 22. Lees-Miller, S. Two human 90-kDa heat shock proteins are phosphorylated *in vivo* at
362 conserved serines that are phosphorylated *in vitro* by casein kinase II. *J Biol Chem*
363 (1989).
364 23. Diezmann, S., Michaut, M., Shapiro, R. S., Bader, G. D. & Cowen, L. E. Mapping the
365 Hsp90 genetic interaction network in *Candida albicans* reveals environmental
366 contingency and rewired circuitry. *PLoS Genet* **8,** e1002562 (2012).
367 24. Bruno, V. M. Regulation of azole drug susceptibility by *Candida albicans* protein
368 kinase CK2. *Mol Microbiol* **56,** 559–573 (2005).
369 25. Cowen, L. E. & Lindquist, S. Hsp90 potentiates the rapid evolution of new traits: drug
370 resistance in diverse fungi. *Science* **309,** 2185–2189 (2005).
371 26. Ewald, P. W.1983. Host-parasite relations, vectors, and the evolution of disease
372 severity. *Ann Rev Ecol Syst* **14,** 465–485 (1983).

373 27. Pearl, L. H. & Prodromou, C. Structure and mechanism of the Hsp90 molecular
374 chaperone machinery. *Annu Rev Biochem* **75,** 271–294 (2006).
375 28. Ali, M. M. U. *et al.* Crystal structure of an Hsp90–nucleotide–p23/Sba1 closed
376 chaperone complex. *Nature* **440,** 1013–1017 (2006).
377 29. Bustamante, C. D., Townsend, J. P. & Hartl, D. L. Solvent accessibility and purifying
378 selection within proteins of *Escherichia coli* and *Salmonella enterica*. *Mol Biol Evol*
379 **17,** 301–308 (2000).
380 30. Blackwell, M. The Fungi: 1, 2, 3 … 5.1 million species? *Am J Bot* **98,** 426–438 (2011).
381 31. Burt, E. T. *et al.* Isolation and partial characterization of Hsp90 from *Candida*
382 *albicans*. *Ann Clin Lab Sci* **33,** 86–93 (2003).
383 32. Mollapour, M. *et al.* Threonine 22 phosphorylation attenuates Hsp90 interaction with
384 cochaperones and affects its chaperone activity. *Mol Cell* **41,** 672–681 (2011).
385 33. Röhl, A., Rohrberg, J. & Buchner, J. The chaperone Hsp90: changing partners for
386 demanding clients. *Trends Biochem Sci* **38,** 253–262 (2013).
387 34. Nathan, D. F. & Lindquist, S. Mutational analysis of Hsp90 function: interactions with
388 a steroid receptor and a protein kinase. *Mol Cell Biol* **15,** 3917–3925 (1995).
389 35. Saville, S. P., Lazzell, A. L., Monteagudo, C. & Lopez-Ribot, J. L. Engineered control
390 of cell morphology *in vivo* reveals distinct roles for yeast and filamentous forms of
391 *Candida albicans* during infection. *Eukaryot Cell* **2,** 1053–1060 (2003).
392 36. Lagree, K. & Mitchell, A. P. Fungal biofilms: Inside out. *Microbiol Spectr* **5,** 1–22
393 (2017).
394 37. Azadmanesh, J., Gowen, A. M., Creger, P. E., Schafer, N. D. & Blankenship, J. R.
395 Filamentation involves two overlapping, but distinct, programs of filamentation in the
396 pathogenic fungus *Candida albicans*. *G3 (Bethesda)* **7,** 3797–3808 (2017).
397 38. Lyons, N. *et al.* Tobacco Hornworm (*Manduca sexta*) caterpillars as a novel host
398 model for the study of fungal virulence and drug efficacy. *Virulence* **11,** 1075–1089
399 (2020).
400 39. Mollapour, M., Tsutsumi, S., Kim, Y. S., Trepel, J. & Neckers, L. Casein kinase 2
401 phosphorylation of Hsp90 threonine 22 modulates chaperone function and drug
402 sensitivity. *Oncotarget* **2,** 407–417 (2011).
403 40. Rehn, A. *et al.* A methylated lysine is a switch point for conformational
404 communication in the chaperone Hsp90. *Nat Commun* **11,** 1–14 (2020).
405 41. Nussinov, R., Tsai, C.-J., Xin, F. & Radivojac, P. Allosteric post-translational
406 modification codes. *Trends Biochem Sci* **37,** 447–455 (2012).
407 42. Robbins, N., Leach, M. D. & Cowen, L. E. Lysine deacetylases Hda1 and Rpd3
408 regulate Hsp90 function thereby governing fungal drug resistance. *Cell Reports* **2,** 878–
409 888 (2012).
410 43. Willger, S. D. *et al.* Analysis of the *Candida albicans* phosphoproteome. *Eukaryot Cell*
411 **14,** 474–485 (2015).
412 44. Ghorai, P., Irfan, M., Narula, A. & Datta, A. A comprehensive analysis of *Candida*
413 *albicans* phosphoproteome reveals dynamic changes in phosphoprotein abundance
414 during hyphal morphogenesis. *Appl Microbiol Biotechnol* **102,** 1–13 (2018).
415 45. Bar-Yosef, H. *et al.* A global analysis of kinase function in *Candida albicans* hyphal
416 morphogenesis reveals a role for the endocytosis regulator Akl1. *Front Cell Infect*
417 *Microbiol* **8,** 1538–13 (2018).
418 46. Vlastaridis, P. *et al.* The pivotal role of protein phosphorylation in the control of yeast
419 central metabolism. *G3 (Bethesda)* **7,** 1239–1249 (2017).
420 47. Cao, C. *et al.* Global regulatory roles of the cAMP/PKA pathway revealed by
421 phenotypic, transcriptomic and phosphoproteomic analyses in a null mutant of the
422 PKA catalytic subunit in *Candida albicans*. *Mol Microbiol* **105,** 46–64 (2017).

48. Soroka, J. *et al.* Conformational switching of the molecular chaperone Hsp90 via regulated phosphorylation. *Mol Cell* **45,** 517–528 (2012).
49. Pereira, F. *et al.* Effect of Sec61 interaction with Mpd1 on endoplasmic reticulum-associated degradation. *PLoS ONE* **14,** e0211180–19 (2019).
50. Mezulis, S., Yates, C. M., Wass, M. N., Sternberg, M. J. E. & Kelley, L. A. The Phyre2 web portal for protein modeling, prediction and analysis. *Nat Protoc* 1–14 (2019).
51. Schrödinger, L. L. C. The PyMOL Molecular Graphics System.
52. Larsson, A. AliView: a fast and lightweight alignment viewer and editor for large datasets. *Bioinformatics* **30,** 3276–3278 (2014).
53. Edgar, R. C. MUSCLE: multiple sequence alignment with high accuracy and high throughput. *Nucleic Acid Res* **32,** 1792–1797 (2004).
54. Kumar, S., Stecher, G., Li, M., Knyaz, C. & Tamura, K. MEGA X: Molecular Evolutionary Genetics Analysis across computing platforms. *Mol Biol Evol* **35,** 1547–1549 (2018).
55. Maddison, W. P. & Maddison, D. R. Mesquite: a modular system for evolutionary analysis.
56. Mersondavies, L. A. & Odds, F. C. A morphology index for characterization of cell-shape in *Candida albicans*. *J Gen Microbiol* **135,** 3143–3152 (1989).
57. Schneider, C. A., Rasband, W. S. & Eliceiri, K. W. NIH Image to ImageJ: 25 years of image analysis. *Nat Methods* **9,** 671 EP –
58. Saldanha, A. J. Java Treeview - extensible visualization of microarray data. *Bioinformatics* **20,** 3246–3248 (2004).
59. Sherry, L. *et al.* Biofilms formed by *Candida albicans* bloodstream isolates display phenotypic and transcriptional heterogeneity that are associated with resistance and pathogenicity. *BMC Microbiol* **14,** 182 (2014).
60. Erlandsen, S. L., Kristich, C. J., Dunny, G. M. & Wells, C. L. High-resolution visualization of the microbial glycocalyx with low-voltage scanning electron microscopy: Dependence on cationic dyes. *J Histochem Cytochem.* **52,** 1427–1435 (2016).

454 **Methods**

455 **Strains, strain construction and culture conditions.** All strains used in this study are listed
456 in Table S1. A detailed description of strain and plasmid construction can be found in the
457 Supplementary Information together with Tables S2 and S3, which list the necessary primers.
458 In preparation for experiments, strains were grown for 16-18 hours in YPM (1% yeast extract,
459 2% peptone, 2% maltose) at 30˚C while shaking at 200 rpm, unless specified otherwise. To
460 repress the *HSP90* wild-type allele, strains were grown in YPD (1% yeast extract, 2%
461 peptone, 2% dextrose) at the temperatures specified. For long-term storage, strains were
462 maintained at -80˚C in 25% glycerol.

463 **Identification of the S530 phosphorylation site.** The S530 phosphorylation site in Hsp90
464 was identified by mass spectrometric analysis of purified Hsp90 in the Proteomics Core
465 Facility at EMBL Heidelberg, Germany. To purify Hsp90 from CK2 deletion mutants
466 (YSD692, YSD675, YSD694, YSD696) and the corresponding wild type (YSD673), strains
467 were grown to mid-log phase at 30˚C in 200 ml volumes in YPD at 30˚C. Whole cell proteins
468 were extracted as described below and the C-terminally TAP-tagged chaperone was pulled
469 down using IgG agarose beads from lysate containing 20 mg of protein (see below). The
470 protein was eluted in 100 µl 1x sample buffer and heated to 95˚C for 10 minutes prior to
471 loading 30 µl onto a 10% Tris-glycine SDS-PAGE gel for separation. Coomassie-stained gels
472 were imaged and the bands corresponding to Hsp90 were cut out and processed by in-gel
473 digestion[49]. Hsp90's phosphorylation sites were identified using Glu-C and trypsin digestion
474 and liquid chromatography-mass spectrometry on a QExactive plus mass spectrometer
475 (Thermo Fisher).

476 **Structural modelling.** A model of the full-length *C. albicans* Hsp90 monomer was generated
477 based on the *S. cerevisiae* Hsp90-Sba1 crystal structure[28] (PDB #2cg9) using the Phyre[2]
478 engine[50]. The model was aligned to the *S. cerevisiae* sequence and visualized using the
479 PyMOL Molecular Graphics System[51].

480 **Ancestral character state reconstruction.** Sequences of 240 fungal taxa were obtained from
481 the Ensembl Genomes database for fungi and aligned with the murine homolog Hsp90ab1
482 (Table S4) in AliView version 1.26[52] using the integrated default alignment program
483 MUSCLE[53]. A Neighbor Joining tree was built in MEGA version 10.1.8[54] and loaded into
484 Mesquite version 3.61[55] for ancestral character state reconstruction using the parsimony
485 criterion.

486 **Western blotting and co-immunoprecipitations.**

487 To determine Hsp90 stability in the wild-type, *MAL2-HSP90* control and hsp90 mutant
488 strains, stationary phase cells grown in YPM were inoculated into YPD or YPM at an OD_{600}
489 of 0.2 and incubated until they reached a log-phase OD_{600} between 1.3 to 1.9 (approximately
490 4.5 hours). 50 ml of cell culture were pelleted, snap frozen in liquid nitrogen, and stored
491 overnight at -20˚C. Pellets were thawed on ice, washed twice with 1x PBS and resuspended in
492 250 µl lysis buffer (50 mM HEPES pH 7.5, 150 mM NaCl, 5 mM EDTA, 1% Triton X100, 1
493 cOmplete EDTA-free protease inhibitor tablet, 1 mM PMSF). Cells were transferred to
494 Precellys 2 ml Tough Micro-organism Lysing Kit tubes (VK05) and lysed using a Precellys
495 Evolution tissue homogenizer. Samples were processed in 3 cycles, each consisting of bead
496 beating at 6,000 rpm for 1 minute, pause for 30 seconds, bead beating at 6,000 rpm for 1
497 minute. Tubes were rested on ice for at least 1 minute between each cycle. Lysates were
498 cleared twice by centrifugation at 20,000 *x*g at 4˚C for 30 minutes, and 5 minutes.
499 Supernatants were transferred to microfuge tubes and refrigerated in preparation for sample
500 preparation and gel loading. The lysates' whole cell protein concentrations were determined
501 with a Quick Start Bradford Protein Assay (Bio-Rad) and calibrated against a BSA standard
502 curve. Samples were diluted to 0.1 µg/µl protein in sample buffer (70 mM Tris-HCl pH 6.8,
503 11.1% glycerol, 1.1% SDS, 0.005% bromophenol blue, 10% 2-mercaptoethanol, all final
504 concentrations), heated at 95˚C for 10 minutes and either cooled on ice prior to loading or
505 stored at -20˚C.

506 As loading controls, 100 µl per sample were loaded onto a 10% SDS-PAGE gel and
507 separated for 20 minutes at 90 volts, followed by 100 minutes at 120 volts. To visualize
508 proteins, gels were stained with SimplyBlue SafeStain (Invitrogen) according to the
509 manufacturer's instructions and imaged by scanning.

510 For immunoblotting of *C. albicans* Hsp90, 15 µl were loaded on a 10% SDS-PAGE gel
511 and separated for 20 minutes at 90 volts, followed by 100 minutes at 120 volts. Proteins were
512 wet-transferred onto a PVDF membrane (Bio-Rad) for 135 minutes at 300 mA in a Mini-
513 PROTEAN Tetra Vertical Electrophoresis Cell filled with transfer-buffer (2 M glycine, 0.25
514 M Tris-base, 20% methanol). To block free sites, membranes were treated with PBST (1x
515 PBS, 0.1% Tween 20) with 0.1% non-fat milk overnight at 4˚C. The blots were probed for 1
516 hour at room temperature with α-CaHsp90[31] diluted 1:10,000 in PBST with 0.1% milk and
517 washed with 1x PBST prior to probing with α-rabbit antibody-HRP conjugate (BioRad
518 #1705046) for 15 minutes at room temperature. Lastly, blots were washed with 200 ml PBST

519 using the SNAP i.d. 2.0 Protein Detection System (Merck Millipore), incubated with Clarity
520 Western ECL (BioRad), and imaged on the Syngene G:Box transilluminator.

521 To purify Hsp90 for mass-spectrometric analysis and to investigate the effect of Hsp90
522 phospho-mutant alleles on co-chaperone binding, 200 ml of cells were grown as described
523 above, washed twice in 1x PBS and resuspended in 2 ml co-IP lysis buffer (50 mM Tris-HCl
524 pH 7.5, 1% Nonidet P 40 Substitute (Sigma #74385), 0.25% deoxycholate Na, 150 mM NaCl,
525 5 mM EDTA, 1 mM Na_2MoO_4•$2H_2O$, PhosSTOP tablet, cOmplete EDTA-free protease
526 inhibitor tablet, 1 mM PMSF, 1 mM Na_3VO_4, and 10 mM NaF). Cells were transferred to 15
527 ml Precellys sample tubes (VWR BERT KT03961-1-4061), mixed with 1 ml acid-washed
528 glass beads (~400 µm) and mechanically disrupted using a Precellys Tissue Homogeniser.
529 Tubes were agitated three times for one minute with one minute on ice in between. The lysate
530 was cleared by centrifugation at 20,000 *x*g twice for 5 minutes at 4°C and protein
531 concentrations determined using the Bradford assay described above. 7.5 mg of protein were
532 mixed with 100 µl of IgG or α-HA agarose, depending on the strain's genotype, in co-IP
533 washing buffer (50 mM Tris-HCl pH 7.5, 1% Nonidet P 40 substitute, 0.25% deoxycholate
534 Na, 150 mM NaCl, 5 mM EDTA, 1 mM Na_2MoO_4•$2H_2O$, 1 mM PMSF, 1 mM Na_3VO_4, and
535 10 mM NaF) and gently rotated for 2 hours at 4˚C. Following precipitation, the agarose beads
536 were washed carefully 3-5 times with 1 ml co-IP washing buffer before being mixed with 100
537 µl 1x sample buffer (6x sample buffer: 0.35 M Tris HCl, 10% (w/w) SDS, 36% glycerol, 5%
538 2-mercaptoethanol and 0.012% bromophenol blue). Prior to loading, samples were heated at
539 95˚C for 10 minutes and cooled on ice ready for loading or stored at -80˚C. Proteins were
540 separated at 120 volts on size-appropriate SDS-PAGE gels.

541 To visualize epitope-tagged co-chaperones, proteins were wet-transferred onto PVDF
542 membranes for 16 hours at 20 volts in a Mini-PROTEAN Tetra Vertical Electrophoresis Cell
543 filled with transfer-buffer (2 M glycine, 0.25 M Tris-base, 20% methanol). Membranes were
544 blocked with PBST and 5% milk for at least 1 hour at room temperature before being probed
545 with primary and secondary antibodies. To visualize TAP-tagged Sti1, membranes were
546 treated with α-TAP antibody (Open Biosystems #CAB1001). Membranes carrying HA-
547 tagged Cdc37, Aha1 or Sba1 were exposed to α-HA antibody (Invitrogen #71-5500). Both
548 primary antibodies were diluted 1:5,000 in PBST with 0.2% milk and subsequently
549 conjugated with α-rabbit antibody-HRP conjugate (BioRad Immun-Star Goat Anti-Rabbit
550 (GAR)-HRP Conjugate #1705046) diluted 1:5,000. Membranes were incubated in antibody
551 solutions for 15 minutes each and washed at least three times using 1x PBST using the SNAP

552 i.d. 2.0 Protein Detection System. Lastly, proteins were visualized with Clarity Western ECL
553 (BioRad).

554 **Temperature growth profiles.** To assess susceptibility to thermal stress, optical densities of
555 stationary phase cultures were measured at 600 nm and adjusted to 0.1 in 1x PBS and serially
556 diluted two-fold. 4 µl of cell suspension were then spotted onto solid YPD or YPM and plates
557 were incubated at the indicated temperature for 48 hours. Plates were photographed and
558 analyzed visually.

559 **Cellular morphogenesis analysis.** Stationary phase cells grown in YPM at 30˚C were diluted
560 to an optical density of 0.2 in YPD or YPM and grown for 16 hours at 30˚C while shaking at
561 200 rpm. In preparation for microscopy, cells were washed and diluted with 1x PBS to a cell
562 density appropriate for microscopy. Images were collected using the DIC settings on a Nikon
563 Eclipse E8000 microscope with a Nikon Digital Sight DS-5M camera. To calculate the
564 morphology index (MI)[56], a total of 100 cells per strain were randomly selected and their
565 width at the septal junction as well as cell length and maximum diameter measured using
566 ImageJ[57]. The MI for each cell was then presented in scatter plots.

567 **Drug susceptibility assays.** Strains were grown to stationary phase at 30˚C in YPM while
568 shaking at 200 rpm and their optical densities were measured at 600 nm and adjusted to ~10^3
569 cells/100 µl. Fluconazole was diluted in water to a starting concentration of 512 µg/ml and 20
570 µl of drug were mixed with 180 µl YPD or YPM in a 96-well flat bottom dish. The drug was
571 then diluted two-fold in YPD or YPM to cover a gradient ranging from 256 µg/ml to 4 µg/ml.
572 100 µl of cell suspension were added to each well and plates were incubated for 48 hours at
573 25˚C and optical densities recorded at 595 nm. A 5 mM radicicol stock solution (DMSO) was
574 diluted to 50 µg/ml in YPM or YPD. The drug was diluted in either media to the following
575 concentrations: 1, 2, 3, 4, 5, 7.5, 10, 15, 20, and 25 µg/ml and strains inoculated as above. To
576 account for the effects of DMSO alone, strains were also inoculated in 0.0275% DMSO.
577 Plates were incubated for 48 hours at 25˚C in the dark and optical densities recorded at 595
578 nm. Optical density values were normalized to the no treatment column and visualized using
579 Java TreeView version 1.1.6r4[58].

580 **Colony morphology screen.** Wild-type, control and mutant strains were grown overnight in
581 YPM at 30˚C while shaking at 200 rpm. Stationary cultures were then diluted to an optical
582 density of 0.02 at 600 nm and 5 µl of cell suspension spotted onto RPMI, Spider, and
583 synthetic defined media with and without Calcofluor White or Congo Red (Table S5). After

584 incubation at 30˚C for 48 hours colonies were visually scored for appearance as 'smooth',
585 'rough', 'wrinkly', or 'wrinkly with hyphal edge' and photographed.

586 **Biofilm analyses.** In preparation for biofilm analyses, *C. albicans* strains were cultured
587 overnight in YPD at 30˚C while shaking at 150 rpm. Stationary phase cells were centrifuged
588 at 4,400 rpm for 5 minutes, washed with 1x PBS and counted using a Neubauer
589 hemocytometer. To induce biofilm formation, cells were diluted to 10^6 cells/ml in RPMI
590 (Sigma-Aldrich/Merck # R7755) and incubated at 37˚C for 24 hours in flat-bottom 96-well
591 dishes for cell viability and biomass assays or on Thermanox™ coverslips for scanning
592 electron microscopy. Cell viability was assessed by metabolic reduction of resazurin sodium
593 salt (Sigma-Aldrich/Merck #R7017). For the assay, 0.1 g of resazurin was dissolved in 10 ml
594 1x PBS and filter-sterilized. Biofilm wells were washed twice with 1x PBS and filled with
595 100 µl of a 1:1000 dilution of resazurin in RPMI. Plates were incubated at 37˚C for 25
596 minutes and absorbance measured at 570 nm. Upon completion of the resazurin cell viability
597 assay, plates were left to dry overnight and biofilm biomass assessed by staining with 0.05%
598 w/v crystal violet. Upon washing and de-staining with 100% ethanol, biomass was quantified
599 by spectrophotometric measurements at 570 nm in a FluoStar Omega (BMG Labtech)
600 microtitre plate reader[59]. To visualize biofilms grown on coverslips, they were washed once
601 with 1x PBS and fixed overnight at 4˚C in 500 µl of 0.15% w/v Alcian Blue dissolved in 2%
602 para-formaldehyde, 2% glutaraldehyde, and 0.15 M sodium cacodylate. Samples were imaged
603 as described previously[60].

604 **Virulence assays.** To assess if Hsp90 phosphorylation affects virulence, we infected
605 caterpillars of the Tobacco Hornworm *Manduca sexta*[38], a novel invertebrate model of fungal
606 disease. In preparation for virulence assays, *C. albicans* strains were grown overnight in YPD
607 at 30˚C and stationary phase cultures were washed twice with 1x PBS. Cell density was
608 adjusted to 10^8 cells/ml for each strain and groups of ten caterpillars were injected with 100 µl
609 cell suspension per animal or 1x PBS in their left rear proleg. Caterpillars were maintained at
610 37˚C and scored for survival after 16 hours.

611 **Statistical analyses.** All analyses were carried out in R Version 3.6.0 and plotted using
612 ggplot2. To assess the effect of the Hsp90 mutant alleles on cellular morphology, the MIs for
613 samples grown in YPD and YPM were compared with each other using the Mann-Whitney U
614 test. Statistical differences between biofilm cell viability and biomass production were
615 assessed using a linear model of strain versus optical density comparing the mutant strains to

616 the maltose control. Statistical significance of caterpillar survival was assessed using Fisher's
617 exact test.
618

Acknowledgments

We would like to thank Prof Alistair J. P. Brown for comments on the manuscript, Ewan Basterfield and Chris Apark for technical support with the *Manduca* caterpillars, and Profs Julia R. Köhler, Jürgen Wendland, and Malcolm Whiteway for their generous plasmid gifts. This work was funded by MRC grant MR/L018349/1 to SD. JLC was supported by the MRC GW4 'Biomed' Doctoral Training Program.

Author contributions

LA, JLC and SD conceived and designed this study. LA constructed strains, prepared samples for mass spectrometry, conducted Hsp90 stability assays and assessed co-chaperone associations. JLC conducted Hsp90 stability and drug susceptibility assays. UO performed the structural modelling analysis. RW performed Hsp90 phylogenetic analyses and ancestral character state reconstruction. CEW performed *in vivo* assays. HOB analyzed growth, morphology, and biofilm data. CS assisted with mass spectrometric analyses. MB & GR performed and analyzed biofilm formation. SD drafted and edited the manuscript.

Competing interest declaration

The authors declare no competing interests.

Additional information

Supplementary information is available for this paper.

Correspondence and requests for materials should be addressed to SD.

Code availability: All custom code is available from:
https://github.com/hobrien/DiezmannLab/blob/master/T25_analysis.Rmd

Corresponding author: Stephanie Diezmann s.diezmann@bristol.ac.uk

645 **Figures**

Alaalm et al. **Figure 1**

a

T25 S530

Candida albicans	ISQLMSLIIN**T**VYSNKEIFLR ... ITKD-FELEE**S**DEEKAAREKE
Saccharomyces cerevisiae	ITQLMSLIIN**T**VYSNKEIFLR ... ITKD-FELEE**T**DEEKAEREKE
Drosophila melanogaster	IAQLMSLIIN**T**FYSNKEIFLR ... VTKEGLELPE**D**ESEKKKREED
Caenorhabditis elegans	IAQLMSLIIN**T**FYSNKEIFLR ... VTKEGLELPE**T**EEEKKKFEED
Homo sapiens	IAQLMSLIIN**T**FYSNKEIFLR ... VTKEGLELPE**D**EEEKKKQEEK
Arabidopsis thaliana	INQLMSLIIN**T**FYSNKEIFLR ... ATKEGLKLEE**T**DDEKKKKEEL

high similarity (≥90%) low similarity (≥50%) no similarity

b

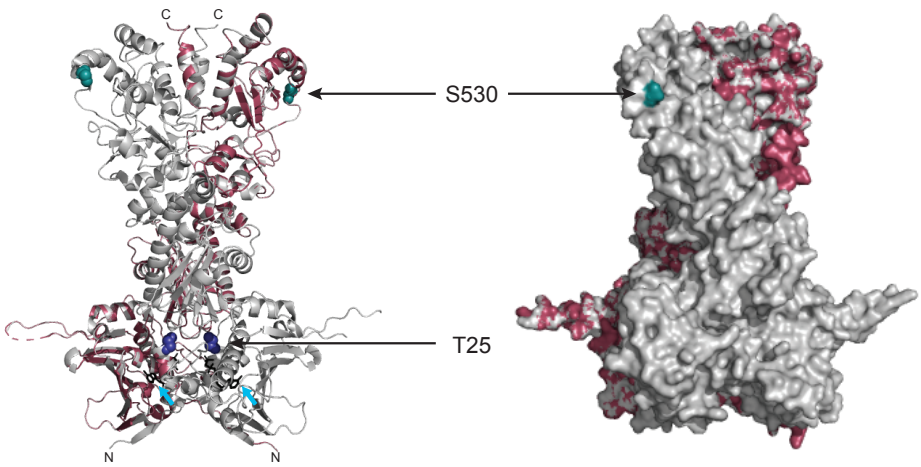

c

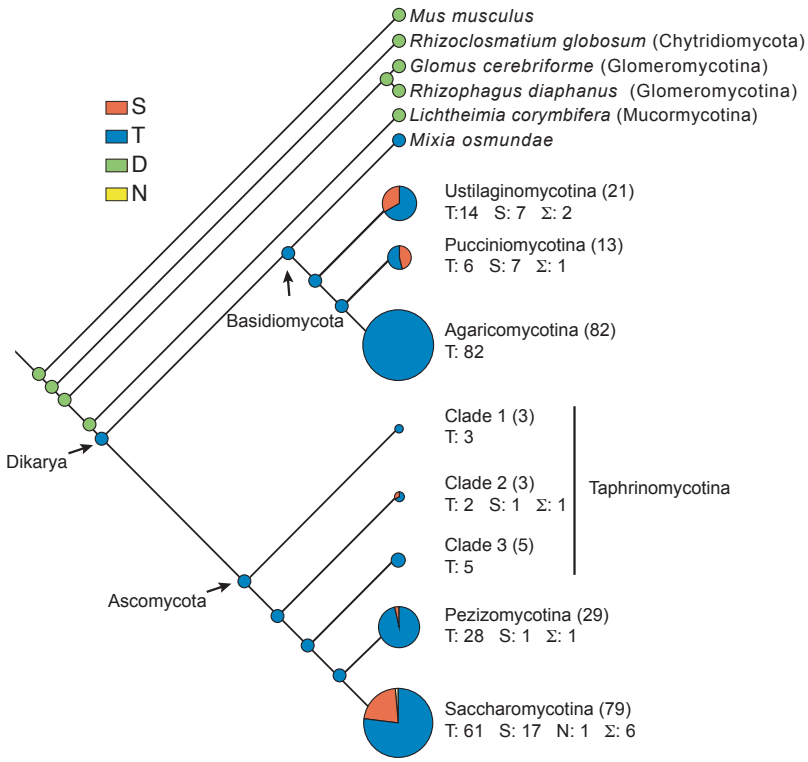

646

647 **Figure 1: Structural modeling and ancestral character state reconstruction of CK2**
648 **phosphorylation sites in Hsp90.** a) Alignment of eukaryotic Hsp90 protein sequences,
649 comparing two fungal sequences to three animal and one plant protein. T25 resides in a
650 highly conserved (red) region of the N-terminal domain of Hsp90. S530 is located in a
651 divergent (blue) region of the Hsp90 middle domain. b) *C. albicans* Hsp90 (purple) modeled
652 on the full-length crystal structure of *S. cerevisiae* Hsp90 (grey). T25 (blue) and S530 (teal)
653 are visualized on the homology model (left) and the surface model (right). Azure arrows point
654 to bound ATP in the homology model. c) Ancestral character state reconstruction of
655 $Hsp90^{S530}$ in 240 fungal taxa reveals at least eleven independent transitions from threonine
656 (blue) to serine (red) within the Dikarya. Basal fungi share the ancestral aspartic acid residue
657 (green) with the animal root (*Mus musculus*) of the tree. Within the Ascomycota and the
658 Basidiomycota, subphyla have been collapsed and the circle size indicates the number of taxa
659 within each clade. The number of taxa per subphylum is given in brackets, and the number of
660 taxa with either threonine or serine or asparagine (yellow) are indicated with T, S, or N. The
661 number of independent transitions within each subphylum is indicated by Σ. For character
662 state reconstruction within ascomycetous and basidiomycetous subphyla see Fig. S1.
663

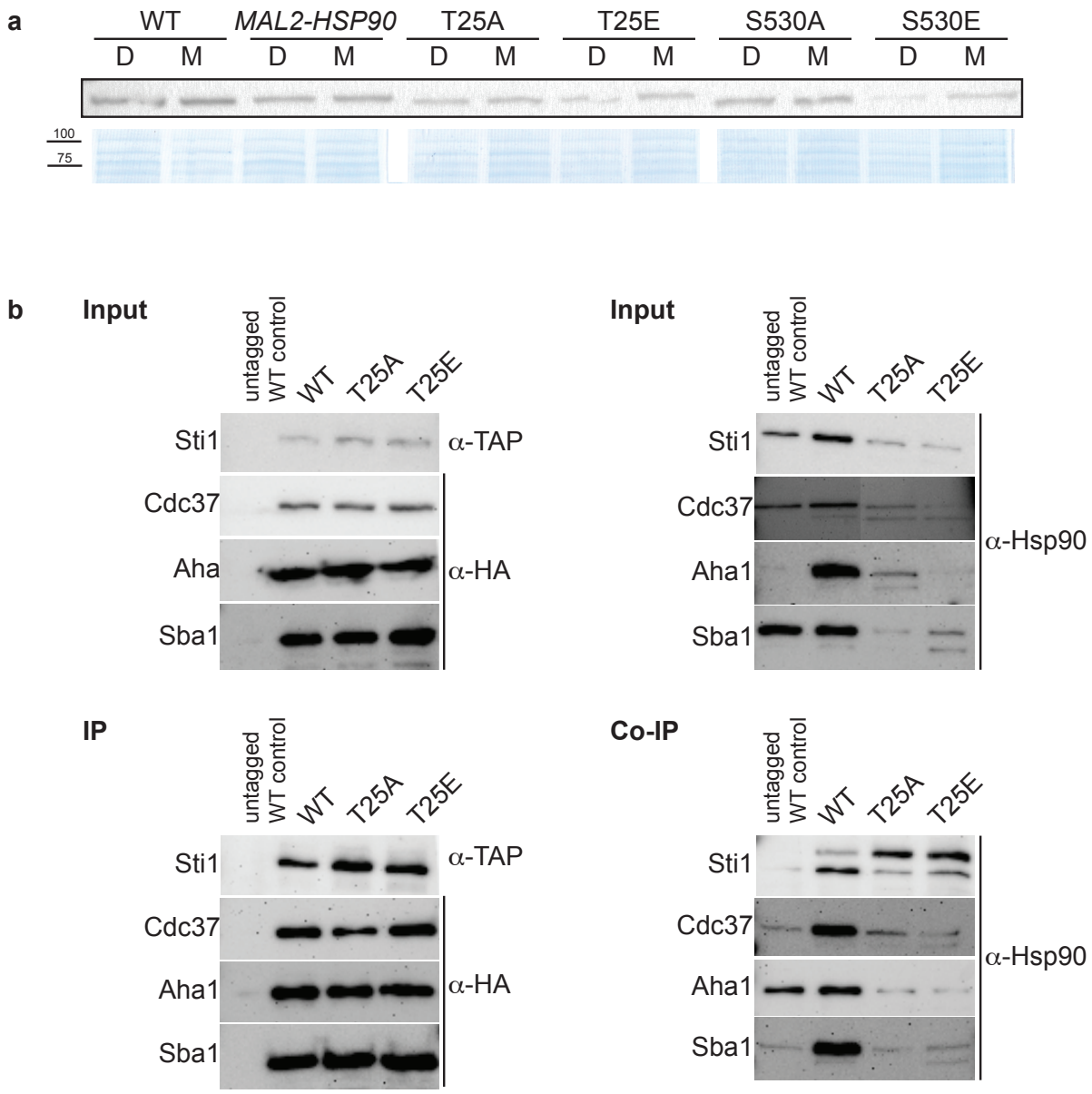

664

665 **Figure 2: The *C. albicans* Hsp90 co-chaperone machinery is regulated by**
666 **phosphorylation.** a) One of two Western blots probed for presence of Hsp90 in *C. albicans*
667 wild-type (WT), promoter control (*MAL2-HSP90*) and T25 and S530 mutant strains (top).
668 Strains were grown in media containing either maltose (M) or dextrose (D) to regulate
669 expression of mutant *HSP90* via the maltose-inducible promoter. A Coomassie-stained SDS
670 gel validates equal loading of protein samples (bottom). b) TAP-tagged Sti1 and HA-tagged
671 co-chaperones Cdc37, Aha1, and Sba1 were co-immunoprecipitated with Hsp90 in the wild
672 type (WT) and the T25 mutants. The input was first probed for presence of co-chaperones and
673 Hsp90 prior to immuno-precipitation with IgG or α-HA agarose targeting the co-chaperones.

674 Levels of co-chaperones were then assessed in the immuno-precipitate (IP) using α-TAP and
675 α-HA antibodies. To screen for co-immunoprecipitated Hsp90 (Co-IP), the membrane was
676 probed with an Hsp90-specific antibody.
677

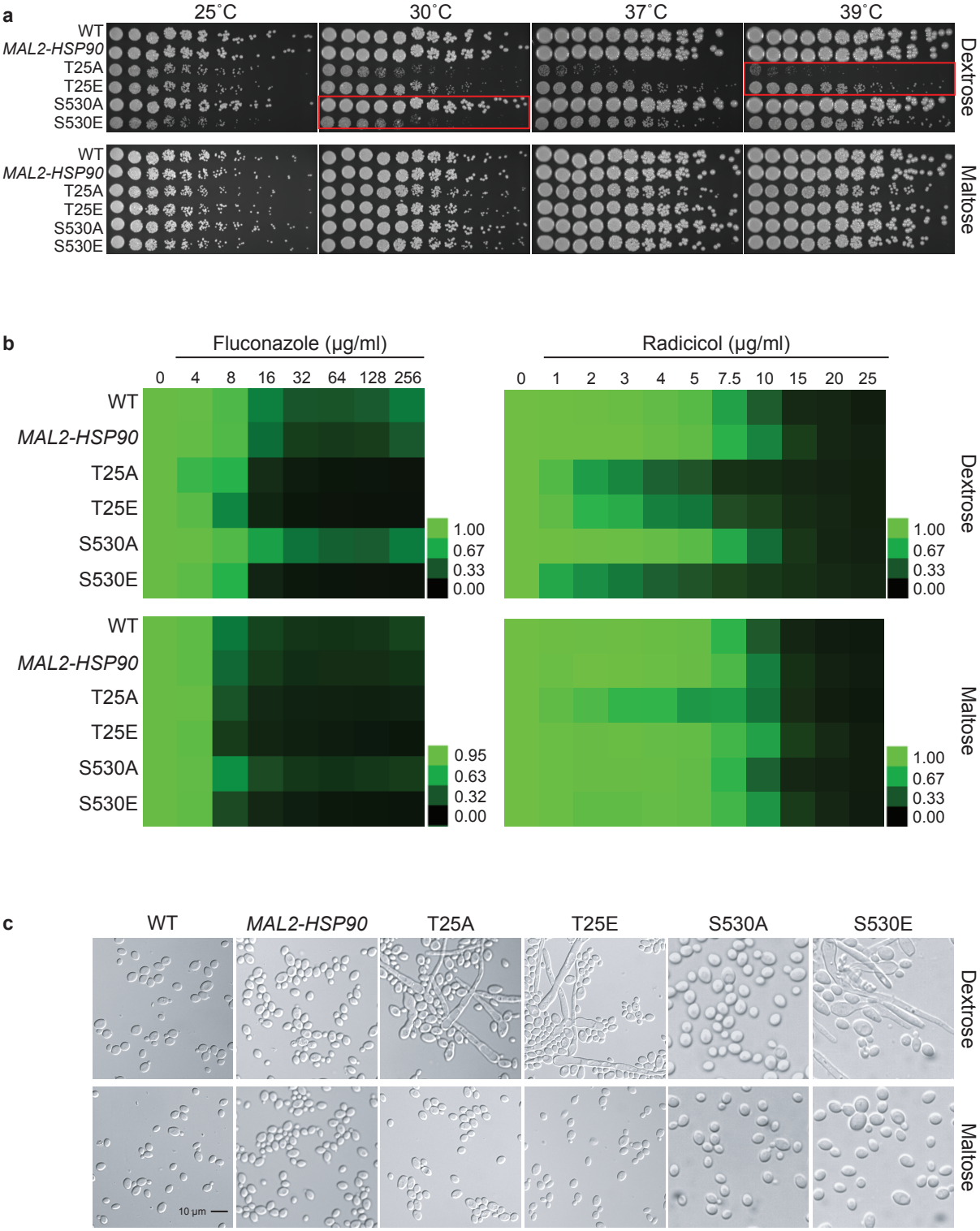

678

679 **Figure 3: Expression of key virulence traits is contingent on Hsp90's phosphorylation**
680 **status.** a) Two-fold serial dilutions of the *HSP90* wild-type, the *MAL2-HSP90* promoter
681 control strain, and *hsp90* phospho-mutants were spotted onto solid media containing either
682 dextrose or maltose and incubated at the indicated temperatures for 48 hours. Red boxes

683 highlighting severe phenotypes. b) Wild-type and mutant cells were exposed to increasing
684 doses of the commonly employed antifungal drug fluconazole and the Hsp90 inhibitor
685 radicicol in media containing either dextrose (top) or maltose (bottom). Following incubation
686 at 25˚C, cell growth was assessed, normalized to the media only control and expressed as heat
687 map where green indicates full growth and black represents no growth. c) DIC microscopic
688 images of representative cells from each strain confirming morphogenetic changes of cells
689 grown in dextrose (top) but not maltose (bottom). Shown are one of two biological replicates.
690

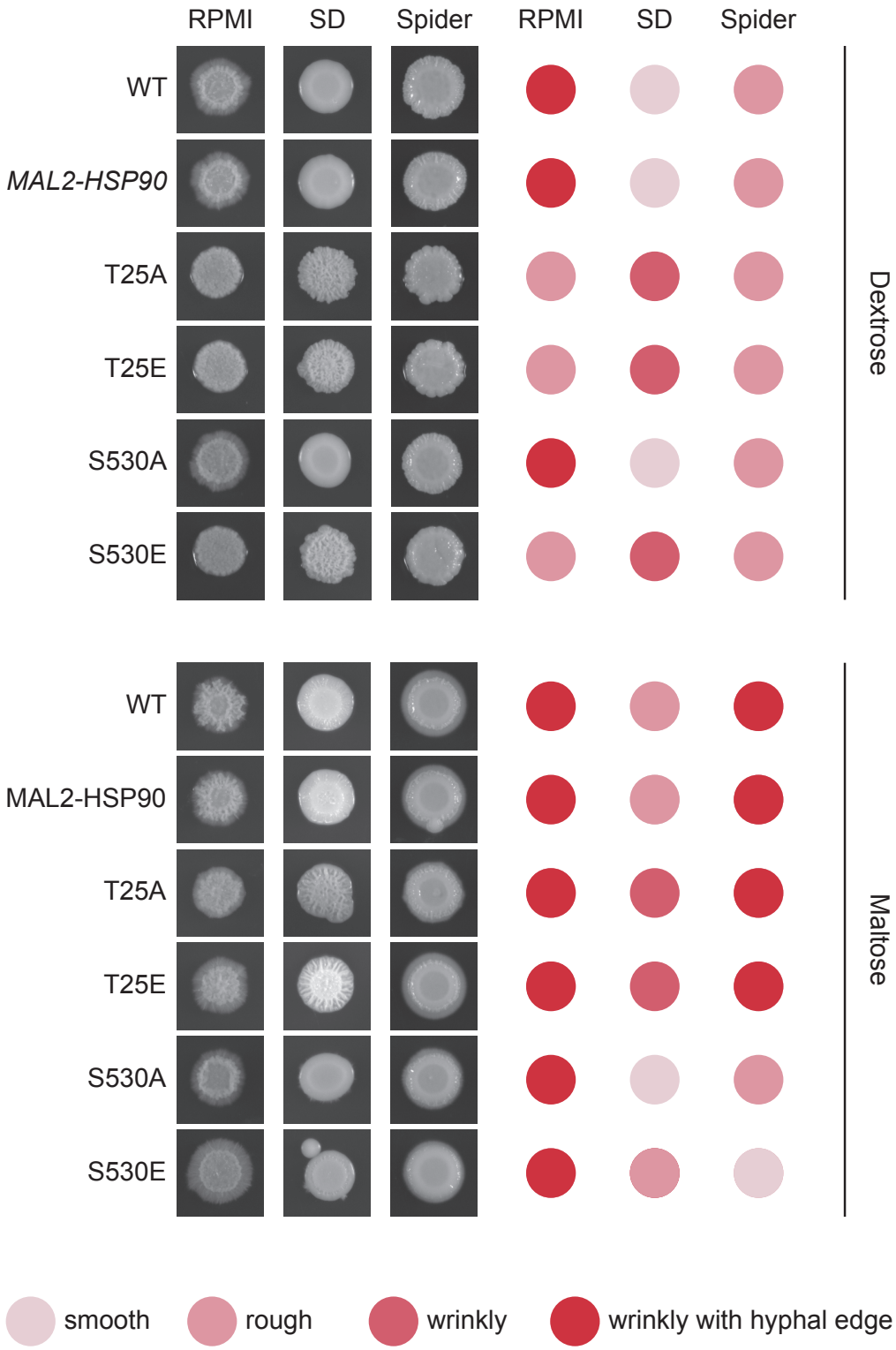

691

692 **Figure 4: Aberrant colony morphology in response to changes in Hsp90 phosphorylation**
693 **patterns.** Images of colonies spotted onto RPMI, Spider or synthetic defined (SD) media
694 containing either dextrose (top) or maltose (bottom). Colonies were scored for their

695 appearance. The darker red the dot, the more extreme the colony phenotype. Shown is one of
696 two replicates.
697

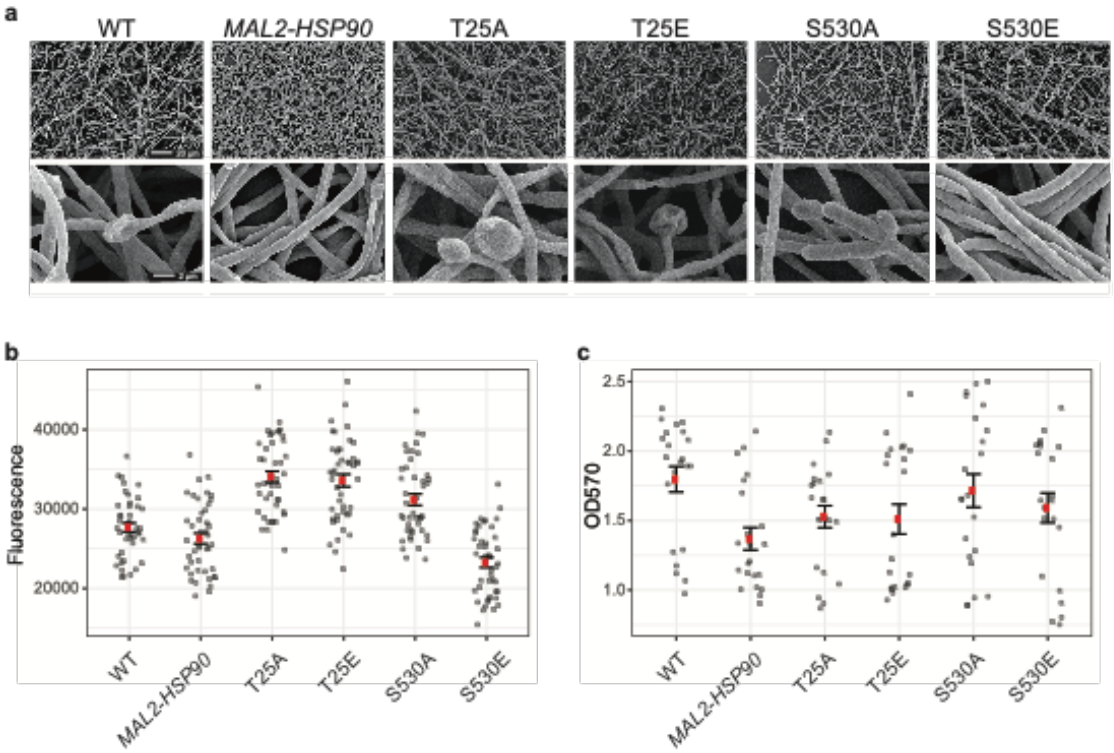

Figure 5: Biofilm architecture remains unaffected by Hsp90 phosphorylation. a) Scanning electron microscopy images of mature biofilms at 800x (top) and 8,000x (bottom) magnification reveal biofilm architecture between the wild type, the control and the phospho-mutants to be indistinguishable upon visual inspection. b) Biofilm cell viability, measured as fluorescence for 44 replicates per strain, is significantly reduced in strain S530E. c) Metabolic biomass measurements for 22 replicates per strain as absorption at OD_{570} were comparable to the promoter control.

707 **Table 1: Patterns of Hsp90 phosphorylation (P) detected in the wild type (WT) and the**
708 **CK2 mutants.**

	C. albicans genotypes				
Hsp90 site	WT	*cka1*Δ/Δ	*cka2*Δ/Δ	*ckb1*Δ/Δ	*ckb2*Δ/Δ
S279	-	P	-	-	-
S294	P	P	P	P	P
S530	P	P	-	P	-

709